Journal of Power Sources 195 (2010) 3365–3373

Contents lists available at ScienceDirect

Journal of Power Sources

journal homepage: www.elsevier.com/locate/jpowsour

Measurement of liquid water content in cathode gas diffusion electrode of polymer electrolyte fuel cell

Kosuke Nishida[a,*], Takeshi Murakami[a], Shohji Tsushima[b], Shuichiro Hirai[b]

[a] Department of Mechanical and System Engineering, Kyoto Institute of Technology, Matsugasaki, Sakyo-ku, Kyoto 606-8585, Japan
[b] Research Center for Carbon Recycling and Energy, Tokyo Institute of Technology, 2-12-1 Ohokayama, Meguro-ku, Tokyo 152-8552, Japan

ARTICLE INFO

Article history:
Received 19 September 2009
Received in revised form 9 December 2009
Accepted 12 December 2009
Available online 24 December 2009

Keywords:
Polymer electrolyte fuel cell
Gas diffusion electrode
Flooding phenomenon
Liquid water content
Visualization

ABSTRACT

Water management in cathode gas diffusion electrode (GDE) of polymer electrolyte fuel cell (PEFC) is essential for high performance operation, because liquid water condensed in porous gas diffusion layer (GDL) and catalyst layer (CL) blocks oxygen transport to active reaction sites. In this study, the average liquid water content inside the cathode GDE of a low-temperature PEFC is experimentally and quantitatively estimated by the weight measurement, and the relationship between the water accumulation rate in the cathode GDE and the cell voltage is investigated. The liquid water behavior at the cathode is also visualized using an optical diagnostic, and the effects of operating conditions and GDL structures on the water transport in the cathode GDE are discussed. It is found that the liquid water content in the cathode GDE increases remarkably after starting the fuel cell operation due to the water production at the CL. At a high current density, the cell voltage drops suddenly after starting the operation in spite of a low water content in the cathode GDE. When the GDL thickness is increased, much water accumulates near the cathode CL and the fuel cell shuts down immediately after the operation. In the final section of this paper, the structure of cathode GDL that has several grooves for water removal is proposed to prevent water flooding and improve fuel cell performance. This groove structure is effective to promote the removal of the liquid water accumulated near the active catalyst sites.

1. Introduction

Polymer electrolyte fuel cell (PEFC) is a promising candidate for mobile and vehicle applications and distributed power systems because of its high power density and low operating temperature. However, there are several technical problems to be solved in an operating PEFC. Especially, water management in the cathode gas diffusion electrode (GDE) composed of the cathode gas diffusion layer (GDL) and catalyst layer (CL) is essential for high performance operation. At a high current density, excessive water generated by the electrode reaction is rapidly condensed in the cathode electrode. When the CL and the open pores inside the GDL are filled with liquid water, oxygen cannot be sufficiently supplied to the reaction sites. This phenomenon known as "water flooding" is critical barrier for high efficiency and high power density. In order to alleviate this issue, it is necessary to understand the liquid water transport through the cathode GDE and optimize the fuel cell design.

Numerical approaches to understand two-phase flow across a cathode electrode of PEFC have been attempted in the previous studies [1–8]. Wang et al. [1] applied a two-phase flow model based on computational fluid dynamics (CFD) to the air cathode of PEFC with a hydrophilic GDL. He et al. [2] and Natarajan and Nguyen [3] proposed two-dimensional two-phase models for PEFCs with interdigitated and conventional flow fields, respectively. Subsequently, Pasaogullari and Wang [4] developed a theory describing liquid water transport in hydrophobic GDL, and explored the effect of GDL wettability on liquid water transport. Recently, Sinha and Wang [5,6], Gostick et al. [7] and Rebai and Prat [8] have developed a pore-network model to understand the liquid water transport in a hydrophobic GDL with the GDL morphology taken into account. While the water transport driven by capillary action was numerically analyzed in detail, the experimental validation of these models was not sufficiently discussed. Many researchers have conducted visualization studies to probe water transport in PEFCs [9–23]. Liquid water formation, transport and removal in cathode flow channel and GDL were investigated by neutron radiography [9–16], X-ray computed tomography [17,18], and optical visualization using transparent fuel cell [19–23]. Boillat et al. [16] resolved the water distribution between the different layers of the membrane electrode assembly (MEA) in an operating PEFC using high-resolution neutron radiography. Sinha et al. [18] have explored the possibility of using X-ray micro-tomography to quantify liquid water distribution along the GDL thickness of a PEFC. Litster et al. [23] developed the fluorescence microscopy technique

* Corresponding author. Tel.: +81 75 724 7321; fax: +81 75 724 7300.
E-mail address: knishida@kit.ac.jp (K. Nishida).

0378-7753/$ – see front matter © 2009 Elsevier B.V. All rights reserved.
doi:10.1016/j.jpowsour.2009.12.073

Nomenclature

A	electrode reaction area (cm^2)
EW	equivalent weight of dry membrane
m_{dry}	weight of dry membrane (g)
m_{MEA}	weight of membrane electrode assembly (g)
m_{PEM}	weight of polymer electrolyte membrane (g)
R_{PEM}	membrane resistance (Ω)
T	cell temperature (°C)
t_{PEM}	membrane thickness (cm)
V_{GDL}	pore volume inside GDL (cm^3)
v_w	specific volume of liquid water ($cm^3\ g^{-1}$)
X_W	average liquid water content in cathode GDE (%)

Greek symbols

λ	water content in membrane
σ	membrane conductivity ($S\,cm^{-1}$)

for visualizing liquid water in hydrophobic fibrous media, and applied to ex situ measurement of water transport in a GDL.

This paper first presents a novel method for quantitatively estimating the average liquid water content inside the cathode GDE of a low-temperature PEFC based on the weight measurement, and investigates the correlation between the water accumulation rate in the porous GDE and the voltage drop of the fuel cell. Although quantitative evaluation of liquid water content in GDL has been conventionally carried out by using neutron radiography [11,12,15,16] and X-ray tomography [18], these equipments for measurement are special and expensive. The measurement method proposed in this study can provide the same information without the use of specialized equipment. Furthermore, the liquid water behavior at the cathode during the fuel cell operation is visualized using an optical diagnostic, and the influences of operating conditions and GDL structures on the water transport through the cathode GDE are also discussed. Finally, the structure of cathode GDL for liquid water removal is proposed in order to prevent water flooding and improve cell performance.

2. Estimation of average liquid water content in cathode GDE

The average liquid water content in the cathode GDE of an operating PEFC can be predicted by measuring the weights of liquid water accumulated in the MEA and polymer electrolyte membrane (PEM). The cathode GDE structurally comprises the cathode GDL and CL. In this experiment, the time-series data of the cell voltage is also measured during the fuel cell operation to investigate the relationship between the water accumulation in the cathode GDE and the voltage change. However, the evaluation of liquid water content in the GDE and the time-series measurement of the cell voltage are conducted at different times, because the assembled cell must be decomposed in measuring the weight of liquid water in the MEA.

The average liquid water content in the cathode GDE, X_W, is defined as the averaged volume fraction of liquid water in the porous media, and given by

$$X_W = \frac{(\Delta m_{MEA} - \Delta m_{PEM})v_w}{V_{GDL}} \times 100 \quad (1)$$

where Δm_{MEA} and Δm_{PEM} are the weight increases of the MEA and PEM due to the liquid water generation, respectively. v_w denotes the specific volume of liquid water, and V_{GDL} the pore volume inside the cathode GDL. The MEA used in this experiment consists of the PEM and two catalyst-coated GDEs. In this study, the liquid water volume in the CLs is neglected because the thickness of CL is very thin and the pore volume is very small. Furthermore, since the anode gas is supplied without humidification, the water condensation in the anode GDE hardly occurs. The water influx to the anode side is only due to the back diffusion through the membrane. Therefore, the liquid water accumulation in the anode GDE can be also ignored. Under these assumptions, the average liquid water content in the cathode GDE including the cathode catalyst layer is described by Eq. (1). Δm_{MEA} is given by measuring the weights of the MEA experimentally before and after operation.

The weight of the PEM, m_{PEM}, in Eq. (1) is estimated by

$$m_{PEM} = m_{dry}\left(\frac{18\lambda}{EW} + 1\right) \quad (2)$$

where m_{dry} is the weight of the dry membrane, λ the water content in the membrane, and EW the equivalent weight of the dry membrane. The water content, λ, is calculated by [24]

$$\lambda = \frac{\sigma}{0.005139}\ \exp\left[1268\left(\frac{1}{273+T} - \frac{1}{303}\right)\right] + 0.63436 \quad (3)$$

where σ is the membrane conductivity and T is the cell temperature. This equation was empirically obtained from measuring the membrane water content and conductivity under a range of water vapor activities at 30 °C. The membrane conductivity, σ, is also given by Eq. (4).

$$\sigma = \frac{t_{PEM}}{R_{PEM} \cdot A} \quad (4)$$

where t_{PEM} is the membrane thickness, R_{PEM} the membrane resistance, and A the electrode reaction area. R_{PEM} is measured by using AC impedance method.

3. Experimental

3.1. Experimental apparatus

Fig. 1 shows the experimental setup, which consists of a constant temperature chamber (Espec, LU-113), a gas supply unit, a high-resolution digital CCD camera (Nikon, Micro-Nikkor lens (105 mm, f/2.8)), a transparent fuel cell, an electronic load (Kikusui, PLZ-164WA), a data logger (Hioki, 8420-50), and a personal computer. The experimental fuel cell equipped with the transparent window is operated in the constant temperature chamber in order to maintain the cell temperature. The CCD camera coupled with the zoom lens for the optical visualization is set outside of the constant temperature chamber, and the working distance (approximately 170 mm) from the cathode channel of the transparent fuel cell is adjusted. The cathode flow field is illuminated by a halogen light

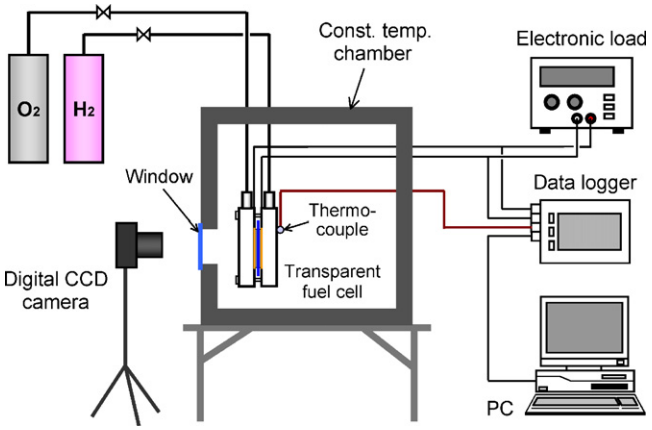

Fig. 1. Experimental setup.

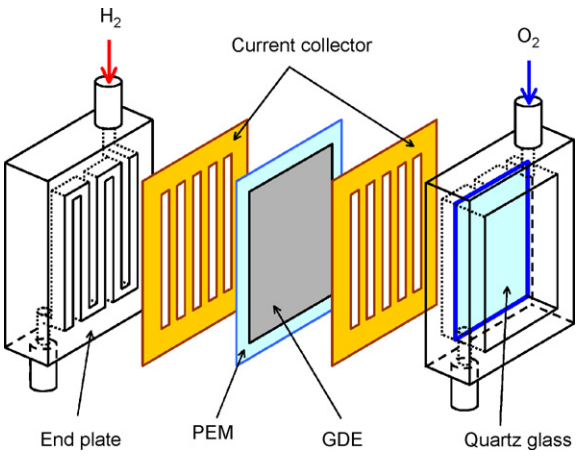

Fig. 2. Schematic diagram of the transparent fuel cell.

source and the close-up images of the GDE surface can be clearly captured. The time-series output voltage and temperature of the operating fuel cell are recorded by the data logger. The cell temperature is measured using a thermocouple. The resistance of the PEM is measured by the LCR meter (HIOKI, 3522-50).

The schematic diagram of the transparent fuel cell is shown in Fig. 2. A PEM (Nafion-115, 127 μm thick) is sandwiched between two hydrophobic GDEs on which platinum particles (0.5 mg cm^{-2}) are loaded as a catalyst layer. The MEA constructed of the PEM and two GDEs is sandwiched between two copper current collector plates (0.5 mm thick) with gold coating. The active electrode area of the experimental fuel cell is 5 cm^2. Two stainless steel end plates with a single-pass serpentine flow channel are placed outside the current collectors. The width, depth and length of the serpentine channel are 2 mm, 3 mm, and 10.5 cm, respectively. In order to observe directly liquid water behavior at the cathode flow field, a quartz glass is inserted into the cathode end plate as a window. Pure hydrogen and oxygen as the fuel and oxidant are fed into the anode and cathode channels at constant flow rates of 30 ml min^{-1} and 60 ml min^{-1}, respectively. Therefore, the utilizations of H_2 and O_2 at 0.3 A cm^{-2} are 0.37 and 0.09. The fuel cell is operated at 20 °C and 1 atm without humidification of the anode and cathode gases. In actual PEFC stacks, high temperature (70–80 °C) and high humidity operations are generally selected. However, water flooding can also be occurred at low-temperature operations such as cold startup and outdoor operation. The conditions in this experiment are valid during these operations of fuel cells.

3.2. Gas diffusion layer

The GDEs used in this experiment were prepared by coating the catalyst ink on three different types of GDL. The properties of the GDLs used are shown in Table 1. TGP-060 and TGP-120 are the paper type GDL produced by Toray. The thickness of TGP-060 is approximately half of that of TGP-120. On the other hand, ELAT is the cloth type GDL produced by E-TEK. The thickness and porosity of ELAT under uncompressed conditions are close to those of TGP-120.

Table 1
Properties of the GDLs.

	Toray TGP-060	Toray TGP-120	E-TEK ELAT LT1400W
Type	Paper	Paper	Cloth
Thickness	190 μm	360 μm	415 μm
Porosity	0.78	0.78	0.75–0.8
Hydrophobicity	PTFE 5 wt%	PTFE 5 wt%	PTFE 5 wt%
MPL	None	None	Coating

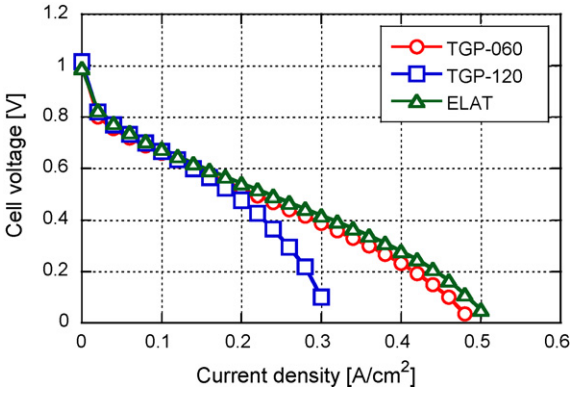

Fig. 3. *I–V* curves for three different types of GDLs (TGP-060, TGP-120 and ELAT LT1400W) at 20 °C.

However, the compressibility of cloth type GDLs tends to be higher as compared with that of paper type GDLs. When the ELAT GDL is compressed in the assembled fuel cell, the thickness is decreased to approximately 180 μm [25]. Since the bulk volume of ELAT is reduced by almost half during the compression, the porosity is also decreased. If the porosity of the uncompressed ELAT is assumed to be 0.75, the porosity of the compressed one is estimated to be 0.42 using the equation offered by Gostick et al. [26]. These values agree with those estimated by Springer et al. [27]. Since the porosity of cloth type GDL is decreased in the assembled cell and the open pores are easily filled with liquid water, the hydrophobic microporous layer (MPL) is coated between the cloth type GDL and CL. This MPL coating is effective in alleviating water flooding near the cathode CL.

Fig. 3 shows the current–voltage (*I–V*) curves for three different type GDLs at 20 °C. The anode and cathode gases are dry H_2 and O_2, respectively. These *I–V* measurements were conducted after the pre-operation of the cell. It is noted that the *I–V* curve for TGP-

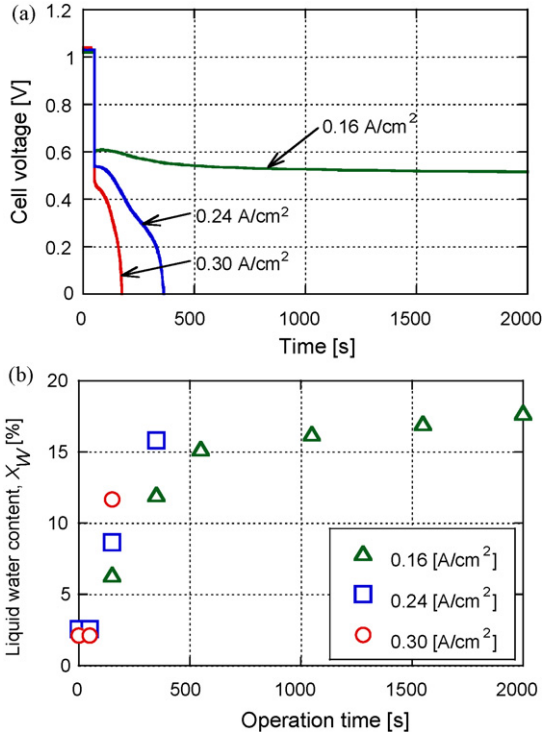

Fig. 4. Characteristics of (a) cell voltage and (b) average liquid water content in cathode GDE at 0.16, 0.24 and 0.3 A cm^{-2}.

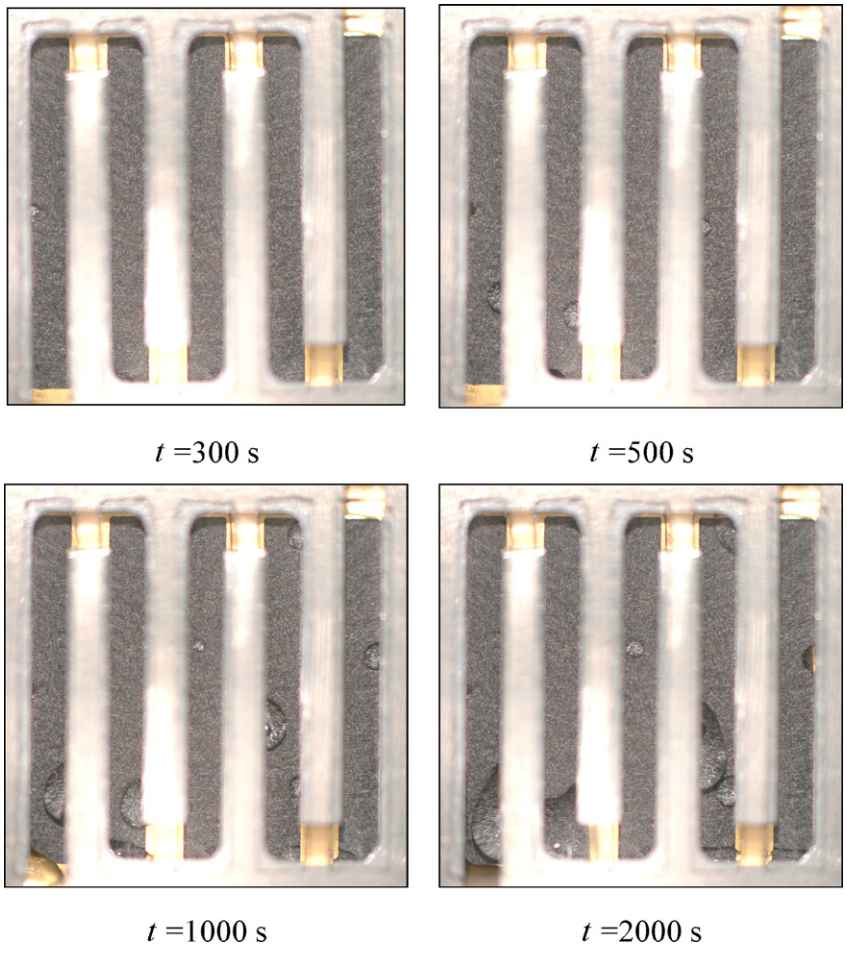

Fig. 5. Images of liquid water behavior on cathode GDE at 0.16 A cm^{-2}.

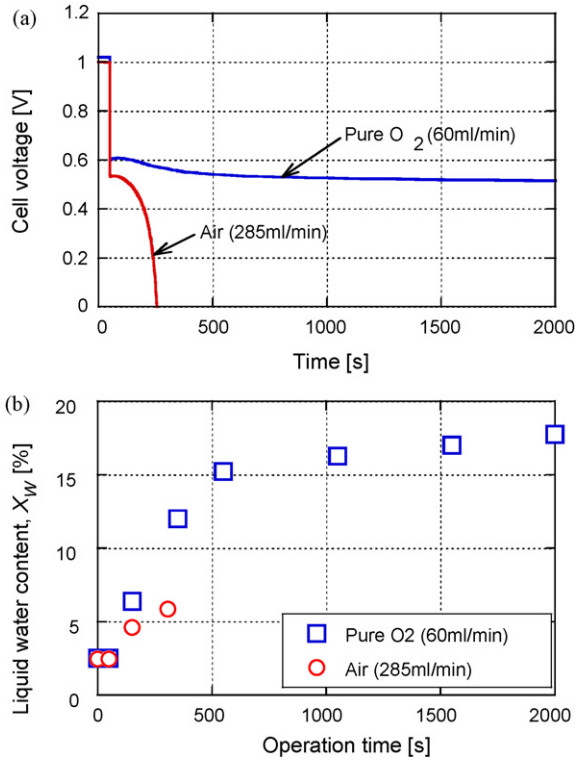

Fig. 6. Characteristics of (a) cell voltage and (b) average liquid water content in cathode GDE at flow rates of pure oxygen 60 ml min^{-1} and air 285 ml min^{-1}.

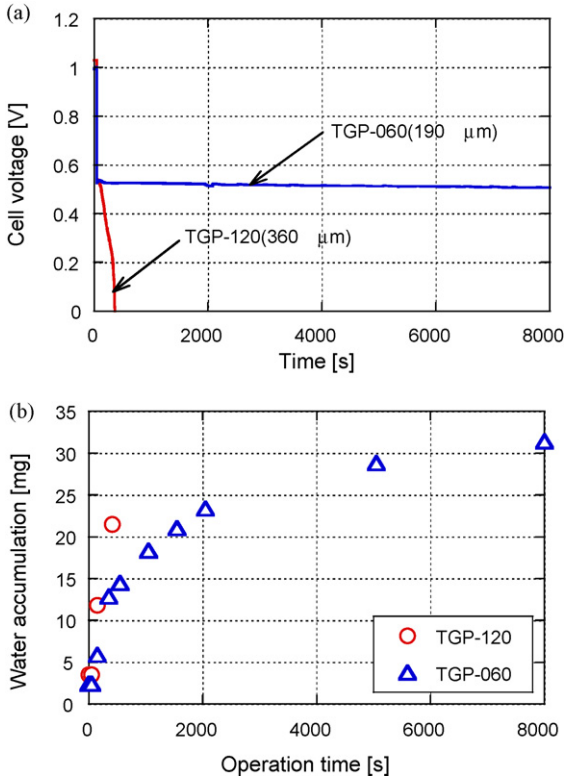

Fig. 7. Effect of GDL thickness on (a) cell voltage and (b) water accumulation in cathode GDE at 0.24 A cm^{-2}.

060 is similar to that for ELAT. However, TGP-120 displays worse performance than TGP-060 and ELAT. In the case of TGP-120, the cell voltage drops remarkably due to the mass transfer limitations when the current density reaches more than 0.2 A cm^{-2}.

3.3. Experimental procedure

The experimental procedure in this study is as follows:

(1) The weight of the dry MEA is measured by the electronic balance (Mettler, AB54). Furthermore, the membrane resistance is also measured by the LCR meter, and the water content in the PEM is predicted before an operation.
(2) The pre-operation of the experimental fuel cell is carried out at 0.16 A cm^{-2} and 20 °C for 2 h in order to hydrate the electrolyte membrane.
(3) After the pre-operation, the assembled fuel cell is decomposed into the MEA, current collectors and end plates, and the weight of the MEA and the membrane resistance are measured. The adherent liquid water on the MEA surface is wiped away before the measurements. Subsequently, the MEA is slowly dried until the liquid water weight in the cathode GDE is adjusted to 3 mg, which is the initial condition. The liquid water weight in the cathode GDE is given by subtracting Δm_{PEM} from Δm_{MEA}.
(4) The constant-current operation test is conducted at 20 °C, and the liquid water behavior at the cathode is directly visualized using the digital CCD camera. The cell voltage change during the operation is also measured.
(5) After the operation test, the experimental cell is decomposed and the weight of the wiped MEA and the membrane resistance are measured again. The average liquid water content in the cathode GDE is evaluated by Eq. (1).

In order to investigate the relationship between the water content in the cathode GDE and the operation time, the operation test (Step 4) and water measurement (Step 5) need to be repeated again and again because the assembled cell must be decomposed in measuring the weight of liquid water in the MEA. After the water measurement in Step 5, we return to Step 3. The wet MEA is reset to the initial state, and the operation test is conducted again.

4. Results and discussion

4.1. Relationship between cell voltage and liquid water content in cathode GDE

PEFC performance is largely influenced by liquid water accumulation in cathode GDL and CL. The characteristics of the cell voltage change and the average liquid water content in the cathode GDE are shown in Fig. 4. The GDL for this experiment is Toray TGP-120 (360 μm thick). The current density as an operating parameter is set to 0.16, 0.24 and 0.3 A cm^{-2}. In all experiments of this study, the fuel cell is held under the open circuit condition for the first 50 s. Fig. 4(a) presents the voltage change during the startup operation. At the

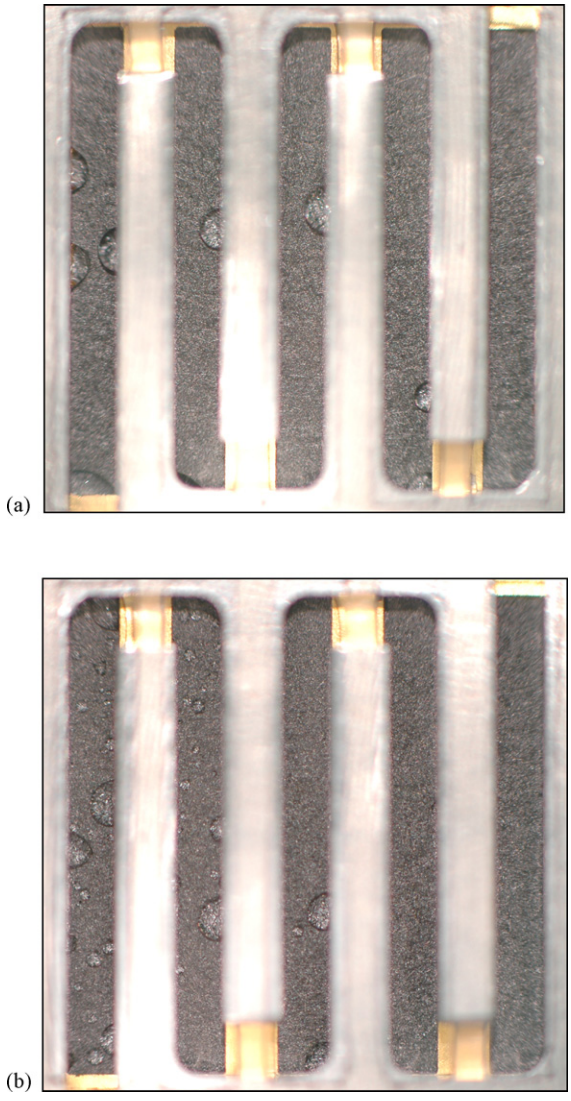

Fig. 8. Images of liquid water behavior on two different thicknesses of GDLs: (a) TGP-120 and (b) TGP-060.

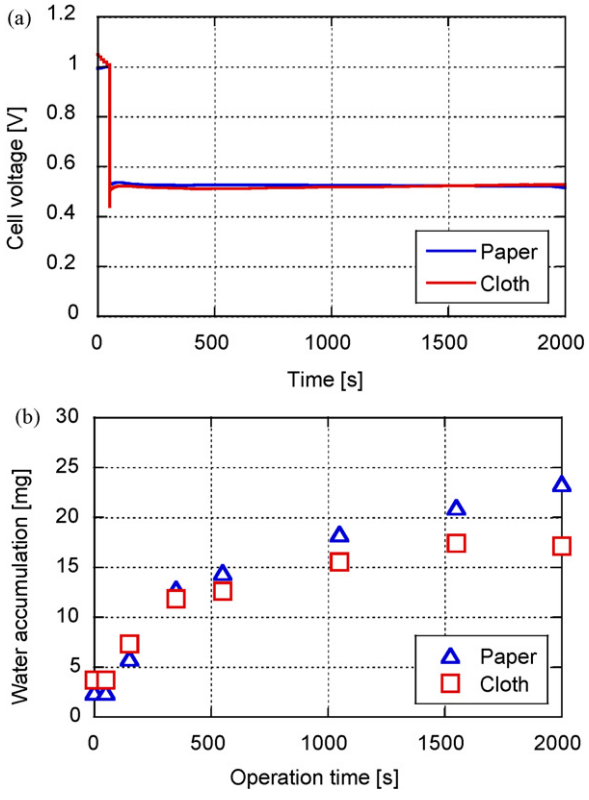

Fig. 9. Comparison of (a) cell voltages and (b) water accumulations in cathode GDE for two different types of GDLs (carbon paper (TGP-060) and carbon cloth (ELAT LT1400W)) at 0.24 A cm^{-2}.

low current density of 0.16 A cm^{-2}, the fuel cell operates stably for 2000 s though the cell voltage decreases a little. When the current density increases up to 0.24 and 0.3 A cm^{-2}, the sudden voltage drop occurs immediately after starting the operation. The relationships between the average liquid water content in the cathode GDE and the operation time are plotted in Fig. 4(b). Since the assembled cell must be decomposed in measuring the weight of liquid water in the MEA, the operation test and water measurement need to be repeated again and again to investigate the relationship between the water content and operation time. After the water measurement, the fuel cell is reset to the initial state and operated again. The plots shown in Fig. 4(b) were obtained from many different operation tests. In the case of 0.16 A cm^{-2}, the liquid water content in the cathode GDE increases rapidly up to approximately 15% for 500 s after starting the operation. After t = 500 s, the rate of increase of the water content slows down because the liquid water accumulated in the cathode GDL is drained to the flow channel. When the current density increases, the rate of increase of the water content in the GDE during the startup increases due to the production of much water. In the cases of 0.24 and 0.3 A cm^{-2}, the cell voltages reduce to zero at t = 400 and 200 s, respectively, though the water content reaches only 16 and 12%. It can be considered that the oxygen transport through the cathode GDL is not limited because of low water content. Therefore, these sudden voltage drops are probably due to the mass transfer limitations inside the CL. If most of the cathode CL is covered with the condensed water, oxygen cannot be sufficiently supplied to the reaction sites and the concentration overpotential is remarkably increased. The amount of liquid water accumulated in the CL tends to increase with an increase in current density.

Fig. 5 shows the sequential images of liquid water behavior on the cathode GDE at the current density of 0.16 A cm^{-2}. The cathode gas (O_2) flows from the upper right to the lower left in the serpentine flow field which has five straight channels. Liquid water is hardly drained from the cathode GDE within 300 s after starting the operation. However, a few liquid droplets accumulated in the cathode GDE appear on the electrode surface at t = 500 s. These droplets on the GDE surface grow and the number of water droplets increases after 500 s of operation. It is noted that the gradual increase of the water content in the cathode GDE after t = 500 s shown in Fig. 4(b) is due to the liquid water removal from the GDE.

4.2. Effect of cathode oxidant on concentration overpotential through GDE

Concentration overpotential through cathode GDE filled with liquid water is associated with oxygen concentration of cathode inlet gas. Fig. 6 shows the effect of cathode oxidant (pure oxygen or

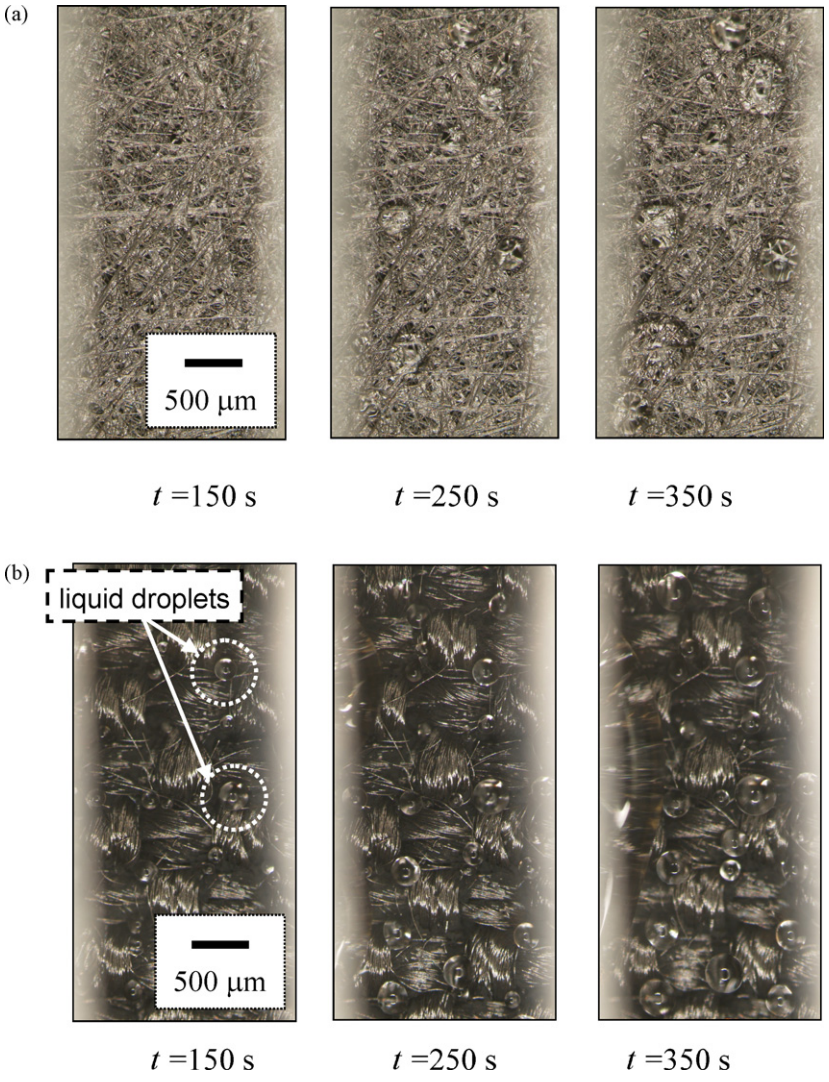

Fig. 10. Sequential images of liquid water behavior on two different types of GDLs: ((a) carbon paper and (b) carbon cloth) during startup.

air) on the cell voltage and average liquid water content in the GDE at 0.16 A cm^{-2}. The GDL for this experiment is Toray TGP-120. The flow rates of pure oxygen and air supplied to the cathode are set to 60 and 285 ml min^{-1}, respectively. Therefore, the utilization of air becomes the same as that of pure oxygen. Fig. 6(a) represents the cell voltage changes during the startup in cases of pure oxygen and air. In the case of pure oxygen, the cell voltage maintains a constant value for 2000 s. On the other hand, the cell voltage for the air flow case decreases immediately after starting the operation because of low oxygen concentration. The average liquid water contents in cathode GDE in both cases are shown in Fig. 6(b). These plots were obtained from several different operation tests. The rate of increase of liquid water content for the air flow case is slower than that for the oxygen flow case because the high flow rate of air suppresses the water condensation inside the cathode GDE. In the case of air flow, although the water content reaches only 6% at t = 350 s, the fuel cell cannot be operated due to the large concentration overpotential.

4.3. Effect of GDL thickness on liquid water accumulation in cathode GDE

Liquid water transport in cathode GDE is also affected by thickness and porous structure of GDL. Fig. 7 shows the effect of GDL thickness on the cell voltage and liquid water accumulation in the cathode GDE at 0.24 A cm^{-2}. In this experiment, two different thickness GDLs (Toray TGP-120 (360 μm thick) and TGP-060 (190 μm thick)) are selected. Fig. 7(a) is the voltage changes for two different GDLs during the startup. In the case of thick GDL (TGP-120), the cell voltage drops suddenly after starting the fuel cell operation. On the other hand, the cell voltage for the thin GDL (TGP-060) case remains constant for 8000 s, because liquid water in the cathode CL and GDL is smoothly removed and oxygen is stably supplied to the reaction sites. The weights of liquid water accumulated in the cathode GDE in both cases are plotted in Fig. 7(b). These plots are obtained from many different operation tests. The rate of the water accumulation for the thin GDL (TGP-060) is slower than that for the thick GDL (TGP-120). This is because the liquid water inside cathode GDE is quickly drained to the flow channel after starting the operation in the case of thin GDL. In the case of thick GDL, the cell voltage decreases to zero at t = 400 s though the weight of liquid water in the GDE reaches only 21 mg. The weight of water of 21 mg is equivalent to the water volume fraction of 15.8% in the GDE. This result indicates that much liquid water tends to remain near the cathode CL in the case of thick GDL.

Fig. 8 shows the images of liquid water behavior on two different thickness GDLs (TGP-120 and TGP-060) at 0.24 A cm^{-2}. These two pictures were taken after 350 s of operation. The cathode gas flows from the upper right to the lower left. In the case of thick GDL (TGP-120), a few liquid droplets are discharged from the corner between the current-collecting ribs and GDL as seen in Fig. 8(a). On the other hand, in the case of thin GDL (TGP-060) shown in Fig. 8(b), many droplets appear not only from the corner between the ribs and GDL but also from the GDL surface. Since the liquid water exhausted from the thin GDL surface is more than that from the thick GDL, the water accumulation rate for the thin GDL slows as shown in Fig. 7(b).

4.4. Comparison of water transport characteristics between paper and cloth type GDLs

Fig. 9 shows the comparison of cell voltages and water accumulations in the cathode GDE for two different types of GDLs (carbon paper (Toray TGP-060) and carbon cloth (E-TEK ELAT LT1400W)) at 0.24 A cm^{-2}. As seen in Fig. 9(a), the cell voltage for the cloth type is almost the same as that for the paper type. The thickness of the compressed cloth GDL in the assembled cell is close to that of the paper GDL (TGP-060). Therefore, in both cases, the dry performances of the fuel cell are similar and the cell voltages at the beginning of the operation are identical. Furthermore, the cell voltages in both cases are constant during the operation despite the water accumulation in the cathode GDE. Under this condition, it is considered that the oxygen transport in the GDL and CL is not limited by the water accumulation because the amount of liquid water accumulated is little. Fig. 9(b) represents the weights of liquid water in the cathode GDE for two types of GDLs. In both cases, the rate of increase of water accumulation slows down after t = 400 s because of the water removal outside the GDE. Furthermore, after 400 s, the

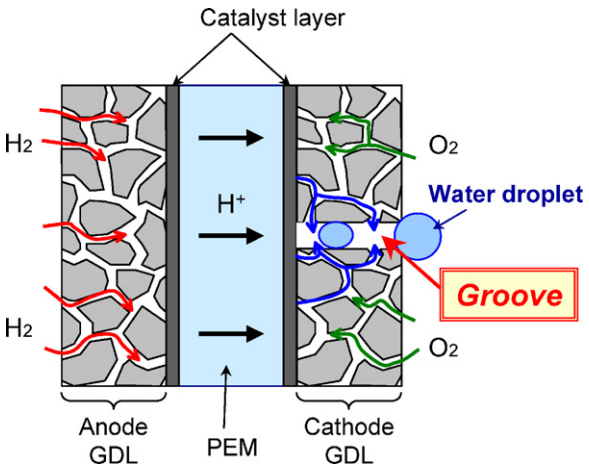

Fig. 11. Structure of cathode GDL with a groove for liquid water removal.

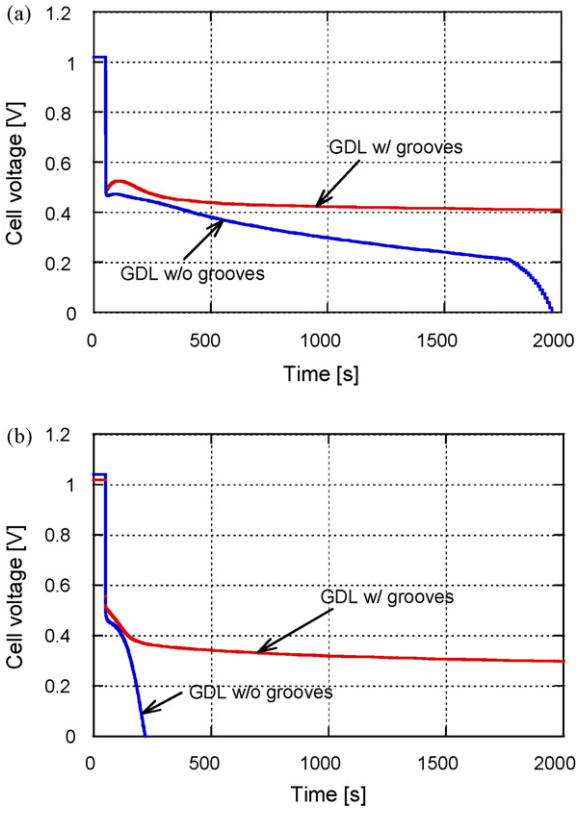

Fig. 12. Effect of groove structure of cathode GDL on cell voltage at cell temperatures of (a) 30 °C and (b) 5 °C.

weight of water in the cathode GDE for the cloth type is less than that for the paper type due to the small pore volume of the compressed cloth GDL. The compressibility of carbon cloth is higher than that of carbon paper. Therefore, when the cloth type GDL is compressed in the assembled fuel cell, the porosity is decreased to be approximately 0.4.

Fig. 10 shows the time-sequential images of liquid water behavior on two different types of GDLs ((a) carbon paper (TGP-060) and (b) carbon cloth (ELAT LT1400W)) during the startup at 0.24 A cm^{-2}. These enlarged pictures were taken at the fifth channel pass in the cathode serpentine flow field which has five straight channels. At t = 150 s after starting the operation, a few small droplets appear on the surface of the cloth type GDL, though liquid water does not exist on the paper type GDL. The total pore volume in the cloth type GDL is smaller than that in the paper type GDL because the thickness of the cloth GDL is decreased by almost half in the assembled cell. Since the amount of liquid water that can exist in the cloth GDL is less than that in the paper GDL, the liquid water inside the cloth is quickly drained to the GDL surface. Furthermore, the number of liquid droplets on the cloth type GDL is more than that on the paper type GDL. This indicates that the transfer paths of liquid water inside the carbon cloth are more than those in the carbon paper.

4.5. Proposal of structure of cathode GDL for liquid water removal

In this study, we propose the structure of cathode GDL which has several grooves for discharging liquid water smoothly and alleviating water flooding. Fig. 11 shows the cross-sectional diagram of the cathode GDL structure with a groove. The groove that is 200 μm wide penetrates completely through the cathode GDL, and the liquid water accumulated near the CL is easily drained into this groove. Gerteisen et al. [28] and Knights et al. [29] have also proposed the hole structures of GDL to aid liquid water transport. Fig. 12 presents the effect of groove structure of cathode GDL on the cell voltage at the cell temperatures of (a) 30 °C and (b) 5 °C. The fuel cell is held under the open circuit condition for the first 50 s, and operated at 0.24 A cm^{-2} after t = 50 s. The GDL for this experiment is Toray TGP-120. The cell performance in the case of thick GDL (TGP-120) without grooves at 30 °C is better than that at 20 °C shown in Fig. 7(a). This is probably because the amount of the condensed water in the GDE decreases with an increase in cell temperature. Three grooves for water removal are positioned within the third, fourth and fifth channels in the cathode serpentine flow field which has five straight channels, as seen later in Fig. 13(a). The length, width and depth of each groove are 18 mm, 200 μm and 360 μm, respectively. At the temperature of 30 °C, the

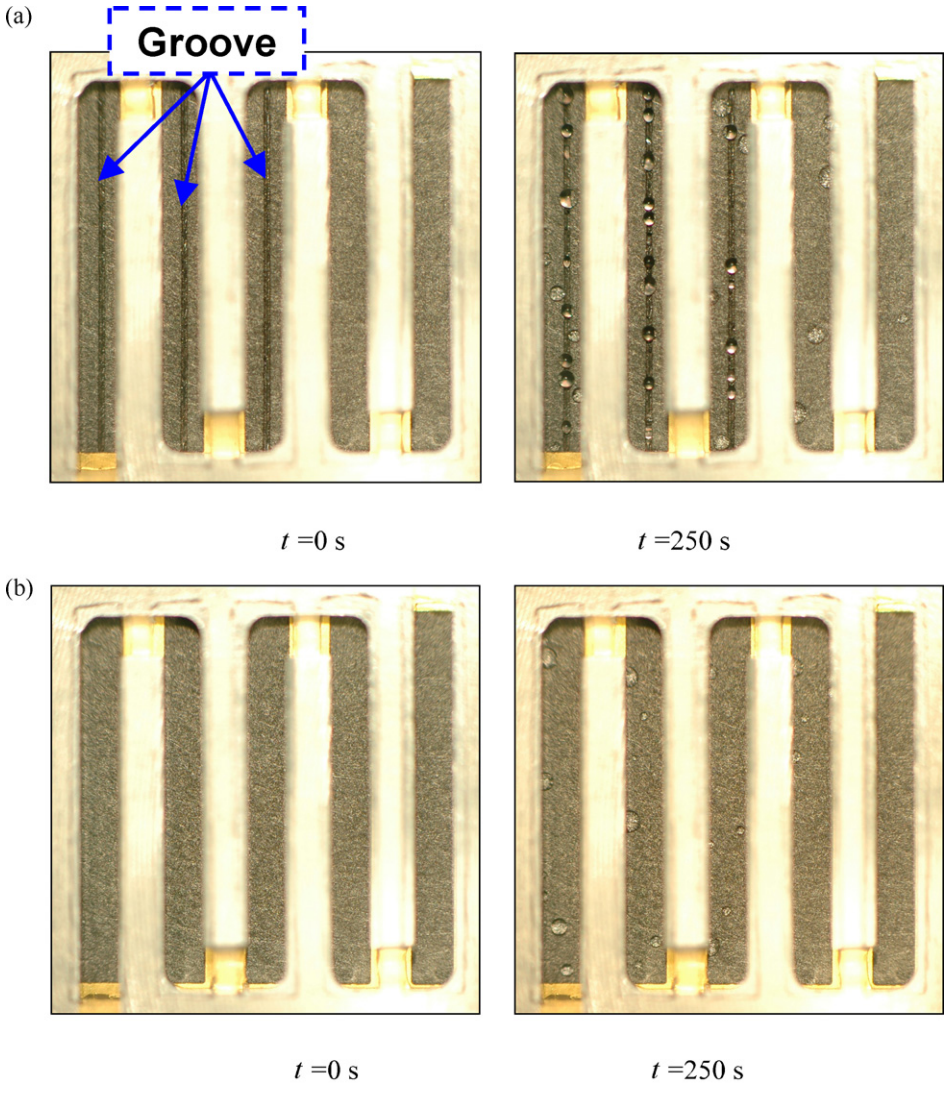

Fig. 13. Images of liquid water removal from cathode GDL (a) with three grooves and (b) without grooves at 0.24 A cm^{-2} and 5 °C.

cell voltage in the case of the cathode GDL with three grooves maintains an almost constant value for 2000 s though the voltage in the case without grooves decreases gradually during the operation. When the cell temperature decreases to 5 °C, the voltage in the case without groove structure drops suddenly after starting the operation because the water condensation occurs remarkably inside the cathode GDE. These results indicate that three grooves installed into the cathode GDL are effective to discharge the liquid water accumulated near the active catalyst sites.

Fig. 13 shows the images of the liquid water removal from the cathode GDL in the cases (a) with three grooves and (b) without grooves. The fuel cell is operated at 0.24 A cm^{-2} and 5 °C, and the paper type GDL (TGP-120) is used. The cathode gas flows from the upper right to the lower left. As shown in Fig. 13(a), three grooves which are 18 mm long, 200 μm wide and 360 μm deep are positioned in the third, fourth and fifth channels of the cathode serpentine flow field. Each groove penetrates completely through the GDL. At t = 250 s, the amount of liquid water discharged from the GDL with three grooves is much more than that without grooves. In the case with groove structure, most of the water droplets are drained from three grooves of the cathode GDL. This suggests that the groove structure of GDL promotes the removal of the liquid water which exists near the cathode CL.

5. Conclusions

In order to understand the water transport through the cathode of a low-temperature PEFC, this paper presented a novel method for quantitatively predicting the average liquid water content inside the cathode GDE based on the weight measurement. The liquid water behavior on the cathode side was also visualized by using an optical diagnostic, and the effects of operating conditions and GDL structures on the cell voltage and the water transport within the GDE were investigated. Furthermore, the groove structure of cathode GDL for water removal was proposed to alleviate the water accumulation near the CL. Especially, the following conclusions can be drawn from this study.

(1) At a low current density, the fuel cell operates stably during the startup and the cell voltage remains almost constant. The rate of increase of the water content in the cathode GDE quickens immediately after starting the operation because of the water generation at the CL. When the liquid droplets begin to drain from the cathode GDE, the rate of increase of the water content slows down. On the other hand, at a high current density, the cell voltage reduces to zero suddenly after starting the operation in spite of a low water content in the cathode GDE.
(2) In the case of air flow at the cathode inlet, the cell voltage decreases immediately after starting the operation due to low oxygen concentration though the water content in the cathode GDE is low.
(3) The rate of water accumulation inside the cathode GDE during the startup decreases with a decrease in GDL thickness. This is because the liquid water in the cathode GDL is rapidly drained to the flow channel in the case of thin GDL. In the case of thick GDL, the cell voltage drops suddenly after starting the operation because of the accumulation of much water near the cathode CL.
(4) The amount of liquid water accumulated in the cathode GDE for the cloth type is less than that for the paper type due to the small pore volume of the compressed cloth GDL. Since the amount of liquid water that can exist in the cloth type GDL is little, the liquid water inside the cloth is quickly drained to the GDL surface.
(5) The groove structure of cathode GDL is effective to remove the liquid water accumulated near the CL. As a result, with this cathode structure, oxygen can be sufficiently supplied to the reaction sites and the cell voltage maintains a constant value.

References

[1] Z.H. Wang, C.Y. Wang, K.S. Chen, J. Power Sources 94 (2001) 40–50.
[2] W. He, J.S. Yi, T.V. Nguyen, AIChE J. 46 (2000) 2053–2064.
[3] D. Natarajan, T.V. Nguyen, J. Electrochem. Soc. 148 (2001) A1324–A1335.
[4] U. Pasaogullari, C.Y. Wang, J. Electrochem. Soc. 151 (2004) A399–A406.
[5] P.K. Sinha, C.Y. Wang, Electrochem. Acta 52 (2007) 7936–7945.
[6] P.K. Sinha, C.Y. Wang, Chem. Eng. Sci. 63 (2008) 1081–1091.
[7] J.T. Gostick, M.A. Ioannidis, M.W. Fowler, M.D. Pritzker, J. Power Sources 173 (2007) 277–290.
[8] M. Rebai, M. Prat, J. Power Sources 192 (2009) 534–543.
[9] R.J. Bellows, M.Y. Lin, M. Arif, A.K. Thompson, D. Jacobson, J. Electrochem. Soc. 146 (1999) 1099–1103.
[10] R. Satija, D.L. Jacobson, M. Arif, S.A. Werner, J. Power Sources 129 (2004) 238–245.
[11] D. Kramer, J. Zhang, R. Shimoi, E. Lehmann, A. Wokaun, K. Shinohara, G.G. Scherer, Electrochem. Acta 50 (2005) 2603–2614.
[12] J. Zhang, D. Kramer, R. Shimoi, Y. Ono, E. Lehmann, A. Wokaun, K. Shinohara, G.G. Scherer, Electrochem. Acta 51 (2006) 2715–2727.
[13] A. Turhan, K. Heller, J.S. Brenizer, M.M. Mench, J. Power Sources 160 (2006) 1195–1203.
[14] M.A. Hickner, N.P. Siegel, K.S. Chen, D.N. McBrayer, D.S. Hussey, D.L. Jacobson, M. Arif, J. Electrochem. Soc. 153 (2006) A902–A908.
[15] K. Yoshizawa, K. Ikezoe, Y. Tasaki, D. Kramer, E.H. Lehmann, G.G. Scherer, J. Electrochem. Soc. 155 (2008) B223–B227.
[16] P. Boillat, D. Kramer, B.C. Seyfang, G. Frei, E. Lehmann, G.G. Scherer, A. Wokaun, Y. Ichikawa, Y. Tasaki, K. Shinohara, Electrochem. Commun. 10 (2008) 546–550.
[17] S.J. Lee, N.Y. Lim, S. Kim, G.G. Park, C.S. Kim, J. Power Sources 185 (2008) 867–870.
[18] P.K. Sinha, P. Halleck, C.Y. Wang, Electrochem. Solid-State Lett. 9 (2006) A344–A348.
[19] K. Tüber, D. Pócza, C. Hebling, J. Power Sources 124 (2003) 403–414.
[20] X.G. Yang, F.Y. Zhang, A.L. Lubawy, C.Y. Wang, Electrochem. Solid-State Lett. 7 (2004) A408–A411.
[21] F.Y. Zhang, X.G. Yang, C.Y. Wang, J. Electrochem. Soc. 153 (2006) A225–A232.
[22] K. Nishida, T. Murakami, S. Tsushima, S. Hirai, Electrochemistry 75 (2007) 149–151.
[23] S. Litster, D. Sinton, N. Djilali, J. Power Sources 154 (2006) 95–105.
[24] T.E. Springer, T.A. Zawodzinski, S. Gottesfeld, J. Electrochem. Soc. 138 (1991) 2334–2342.
[25] S. Escribano, J.F. Blachot, J. Ethève, A. Morin, R. Mosdale, J. Power Sources 156 (2006) 8–13.
[26] J.T. Gostick, M.W. Fowler, M.D. Pritzker, M.A. Ioannidis, L.M. Behra, J. Power Sources 162 (2006) 228–238.
[27] T.E. Springer, T.A. Zawodzinski, M.S. Wilson, S. Gottesfeld, Electrochem. Soc. Proc. 95 (1995) 137–151.
[28] D. Gerteisen, T. Heilmann, C. Ziegler, J. Power Sources 177 (2008) 348–354.
[29] S.D. Knights, K.M. Colbow, J.S. Pierre, D.P. Wilkinson, J. Power Sources 127 (2004) 127–134.